A double constrained robust capon beamforming based imaging method for early breast cancer detection*

Xiao Xia(肖 夏)†, Xu Li(徐 立), and Li Qin-Wei(李钦伟)

School of Electronic Information Engineering, Tianjin University, Tianjin 300072, *China*

(Received 6 January 2013; revised manuscript received 1 February 2013)

Ultra-wideband (UWB) microwave images are proposed for detecting small malignant breast tumors based on the large contrast of electric parameters between a malignant tumor and normal breast tissue. In this study, an antenna array composed of 9 antennas is applied to the detection. The double constrained robust capon beamforming (DCRCB) algorithm is used for reconstructing the breast image due to its better stability and high signal-to-interference-plus-noise ratio (SINR). The successful detection of a tumor of 2 mm in diameter shown in the reconstruction demonstrates the robustness of the DCRCB beamforming algorithm. This study verifies the feasibility of detecting small breast tumors by using the DCRCB imaging algorithm.

Keywords: ultra wideband, early breast cancer detection, double constrained robust capon beamforming algorithm, antenna array

PACS: 41.20.–q, 41.20.Jb, 41.20.Gz, 02.70.Bf **DOI:** 10.1088/1674-1056/22/9/094101

1. Introduction

Breast cancer is becoming one of the primary cancers which are harmful to womens' health. Early detection and timely medical intervention are key factors for long-term survival and increased quality of life of breast cancer patients. X-ray mammography is currently regarded as the most common detection method for early breast tumors.[1–3] Although it provides high-quality images at a relatively low radiation dose for the majority of patients, its inherent weaknesses, such as high false detection rate and impossibility of being a routine detection method, are well recognized. The disadvantages existing in methods such as magnetic resonance imaging (MRI) and computed tomography (CT) restrict them from being effective approaches to early-stage tumor detection.[4–6]

Both tomography and subsurface ultra-wideband (UWB) radar techniques have been proposed for exploiting the dielectric-property contrast between malignant and normal breast tissue. The goal of microwave tomography is to recover the dielectric-property profiles of the breast from the measurements of narrowband microwave signals transmitted through the breast. While promising preliminary clinical results have been reported in Ref. [7], the solution of this nonlinear inverse-scattering problem is challenging and requires an intensive reconstruction algorithm. UWB microwave imaging technology is very attractive for early breast cancer detection since it can provide both the necessary imaging resolution and an adequate penetration depth in the breast. In this technique, a low-power UWB microwave pulse is radiated by an antenna into the breast and penetrates through the skin and travels through the breast to interact with the malignant and other breast tissue. The UWB techniques do not attempt to reconstruct the profile of the breast, but instead seek to identify the presence and location of a tumor.[8–10] The backscattered waveforms which contain the inside information of the breast are captured by the receiving antennas for further image reconstruction of the breast.

In this paper, a three-dimensional (3D) planar breast model for obtaining the data is demonstrated. The microwave propagation in the breast is described by the finite-difference time-domain (FDTD) method.[11–13] The dispersive properties of the normal fatty layer, the skin, the gland, the tumor, and the chest wall are taken into consideration by using the single-pole Debye model to approach the real electrical properties of the breast. In this method, a tumor with a size of 2 mm in diameter is assumed to be embedded in the breast model. The double constrained capon beamforming algorithm (DCRCB) with high robustness is applied to the image reconstruction.

The remainder of this paper is organized as follows. In Section 2, the 3D breast model is presented. In Section 3, the detail of the beamforming algorithm for image reconstruction is described. In Section 4, the simulation results to confirm the correctness of the algorithm are presented. Finally, conclusions are drawn from the present study.

2. System configuration and modeling

Figure 1 shows a 3D geometric configuration of the planar breast structure used in this study. Such a planar breast model is a typical model used in the relevant investigations, which is

*Project supported by the National Natural Science Foundation of China (Grant No. 61271323) and the Open Project from State Key Laboratory of Millimeter Waves, China (Grant No. K200913).

†Corresponding author. E-mail: xiaxiao@tju.edu.cn

© 2013 Chinese Physical Society and IOP Publishing Ltd

assumed to approach the naturally flattened breast of a patient lying in a supine position. The size of the portion of the breast tissue is identified in the model. A tumor with a size of 2 mm in diameter is assumed to be embedded deeply in the breast. And 30 spheres and ellipsoids assumed as glands with different sizes and shapes are randomly added in the model to create a realistic breast and work as noise to verify the robustness of the imaging algorithm. An antenna array composed of 9 antennas is arranged on the surface of the skin, as shown in Fig. 2. During the detection, a Gaussian monocycle pulse (GMP) is alternatively emitted from one antenna and the backscattered waveforms are collected by the other 8 antennas. By repeating this step, 72 group signals are collected and used in the subsequent image reconstruction. The backscattered signals are computed by using the finite-difference time-domain method. Both the dispersive properties and the spatial heterogeneity of normal breast tissue are considered in the FDTD model. The frequency dependences of dielectric constant and conductivity over the band of interest can be accurately modeled by using the following single-pole Debye dispersion equation:[14]

$$\varepsilon_{\mathrm{r}}(\omega) - \mathrm{j}\frac{\sigma(\omega)}{\omega\varepsilon_0} = \varepsilon_\infty + \frac{\varepsilon_{\mathrm{s}} - \varepsilon_\infty}{1 + \mathrm{j}\omega\tau} - \mathrm{j}\frac{\sigma_{\mathrm{s}}}{\omega\varepsilon_0}, \tag{1}$$

where ε_{s} is the static dielectric constant, ε_∞ is the dielectric constant at infinite, and σ_{s} is the static conductivity.

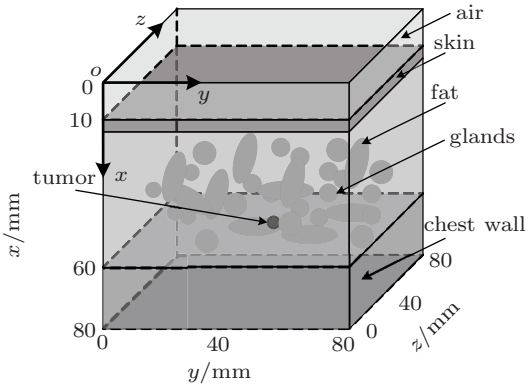


Fig. 1. The 3D breast geometric configuration.

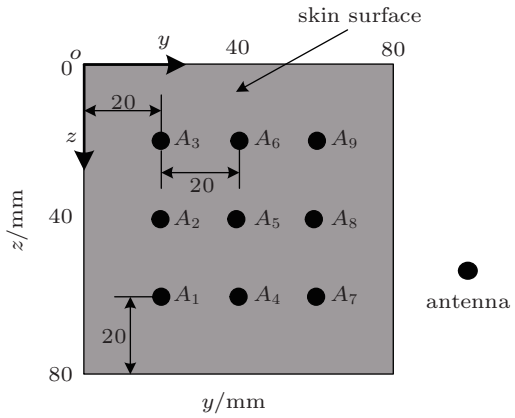


Fig. 2. Layout of the antenna array arranged on the skin surface.

3. Beamforming algorithm for imaging

The reconstructed image is obtained by scanning the whole region of the breast and using a beamformer designed for each scanned location to make the backscattered signals detected at each antenna. In order to present the imaging algorithm, the scan point r is assumed. The beamformer is designed to ensure that the backscattered signals from r have the maximum gain while attenuating signals from other locations.

The GMP signal employed in the breast cancer detection is given by

$$e(t) = -\sqrt{e}\left(\frac{2\pi}{\tau}\right)(t - T_{\mathrm{c}})\exp\left(-\frac{1}{2}\left(2\pi\frac{t - T_{\mathrm{c}}}{\tau}\right)^2\right), \tag{2}$$

where T_{c} is the time shift factor, and τ is the impulse width. The impulse has a central frequency of 5 GHz and a band width of around 9 GHz to ensure the imaging resolution and the adequate penetration depth in the breast.

Figure 3 shows the as-detected signals for which the impulse is emitted from A_1 and the backscattered signals are collected at A_4, A_7, A_8, and A_9, respectively. The tumor with a size of 2 mm in diameter is assumed to be located at (35, 40, 40).

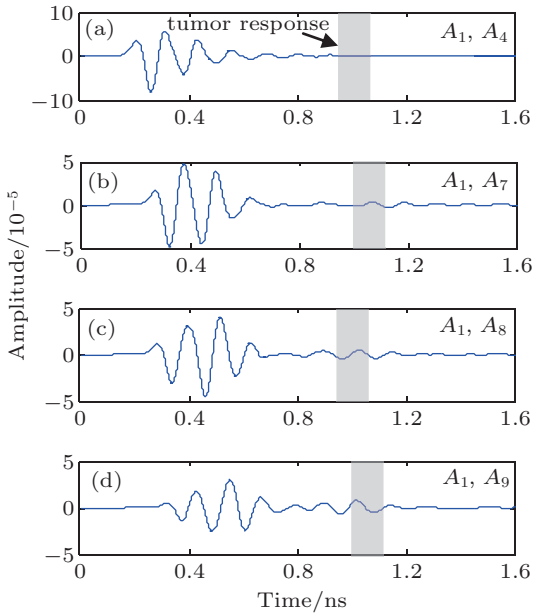


Fig. 3. (color online) As-detected signals, the impulse is emitted from A_1, the signals are detected at (a) A_4, (b) A_7, (c) A_8, and (d) A_9, respectively.

It is obvious that the detected signals contain direct waves, the reflection from the skin, and other scatterings. However, the responses from the gland, the tumor, and the chest wall cannot be observed clearly in this stage due to the abrupt attenuation of signal during propagation. The marked regions in the figure represent the assumed tumor response. The tumor information can be obtained by subtracting the reference signals for the tumor-free cases from the detected signals. Actually, it is a crucial problem to correctly extract the

reference signal of the tumor-free case from the detected signals in a real case. This is very significant in clinical applications. In Ref. [15], a method of extracting the reference signals by using an average algorithm based on the multiple corresponding detections was reported. The extracted signals are qualified to be used as the reference signals of the tumor-free case. The signals after the subtraction process shown in Fig. 4 are employed to create the reconstructed breast image.

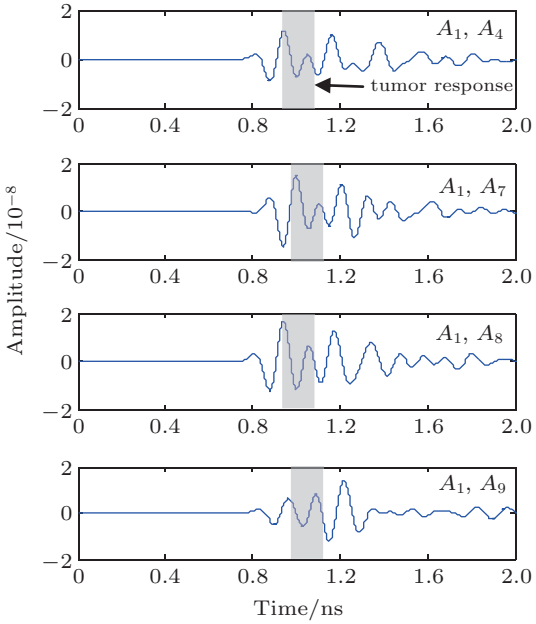


Fig. 4. (color online) Subtracted signals, showing the tumor response, with the impulse emitted from A_1, detected by (a) A_4, (b) A_7, (c) A_8, and (d) A_9, respectively.

For the purpose of designing the beamformer, the detected signals are assumed to contain only the backscattering information from tumor point r. The time for a microwave to propagate through breast tissues from antenna A_i to point r and back to antenna A_j is given by

$$\tau_{i,j}(r) = \frac{1}{\Delta t}(\|r_i - r\|/V + \|r_j - r\|/V), \quad \{i,j \subset (1,9);\ i \neq j\}, \tag{3}$$

where Δt is the sampling interval, which is assumed to be sufficiently small, V is the velocity of the microwave propagating in the breast tissues, i and j are the serial numbers of the antennas, $r_i - r$ is the distance between A_i and the point to be focused at, and $r_j - r$ is the distance between A_j and the point to be focused at. The signals in each channel are delayed by an integer number of $n_{i,j}(r)$ for the purpose of aligning the response from r in time

$$n_{i,j}(r) = n_{\max} - \tau_{i,j}(r), \tag{4}$$

where $n_{\max}$ is the maximum propagation delay over all channels and locations.

In order to maximize the tumor response and minimize the noise, appropriate weighting coefficients should be selected for the superposition of aligned signals. The double constrained robust capon beamforming (DCRCB) algorithm is used in this paper. The cost function of DCRCB is[16,17]

$$\min_{\boldsymbol{a}_s} \boldsymbol{a}_s^{\mathrm{H}} \boldsymbol{R}^{-1} \boldsymbol{a}_s \text{subjectto} \|\boldsymbol{a}_s - \boldsymbol{a}\|^2 \leq \varepsilon_0, \quad \|\boldsymbol{a}_s\|^2 = M, \tag{5}$$

where $\boldsymbol{R}$ is the covariance matrix of the aligned signals, $\boldsymbol{a}_s$ is the real direction of the beamformer, $\boldsymbol{a}$ is the expected direction, and ε_0 is the error of the directions. The principle of DCRCB is to search for the best weighting vector to minimize the power of the expected noise. The direction vector is covered by an ellipsoid to improve the stability of the algorithm. A constant norm constrain is also enforced on the direction vector to improve the signal-to-interference-plus-noise ratio (SINR) during application. As a result of $||\boldsymbol{a}_s||^2 = M$, Eq. (5) can be expressed as

$$\|\boldsymbol{a}_s - \boldsymbol{a}\|^2 \leq \varepsilon_0 \Leftrightarrow \mathrm{Re}\left(\boldsymbol{a}^{\mathrm{H}} \boldsymbol{a}_s\right) \geq M - \varepsilon_0/2. \tag{6}$$

The constrained function can easily turn into an unconstrained optimization problem

$$F(\boldsymbol{a}_s, \lambda, \mu) = \boldsymbol{a}_s^{\mathrm{H}} \boldsymbol{R}^{-1} \boldsymbol{a}_s + \mu\left(2M - \varepsilon_0 - \boldsymbol{a}^H \boldsymbol{a}_s - \boldsymbol{a}_s^H \boldsymbol{a}\right) + \lambda\left(\|\boldsymbol{a}_s\|^2 - M\right). \tag{7}$$

The solution procedure of $\boldsymbol{a}_s$ can be found in Ref. [18], and the weighting vector can be obtained as follows:

$$\boldsymbol{w}_{\mathrm{DCRCB}} = \frac{\boldsymbol{R}^{-1} \boldsymbol{a}_s}{\boldsymbol{a}_s^{\mathrm{H}} \boldsymbol{R}^{-1} \boldsymbol{a}}. \tag{8}$$

The weighted signal, with the impulse emitted from A_1, detected by other antennas shown in Fig. 5, indicates that the tumor response is maximized and the noise is weakened simultaneously.

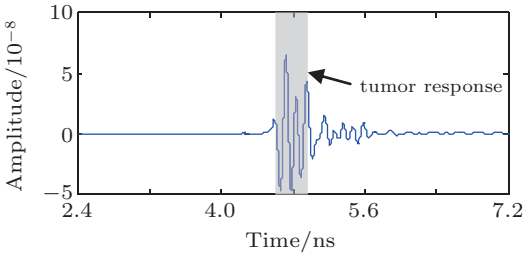


Fig. 5. (color online) Weighted signal, with the impulse emitted from A_1, detected by the other antennas.

The weighted signal $x_i(r)$ is windowed with $h[n]$ to eliminate the effect of clutter. The choice for the window is

$$h[n] = \begin{cases} 1, & n_{\max} \leq n \leq n_{\max} + l, \\ 0, & \text{otherwise}. \end{cases} \tag{9}$$

A tumor with a size of less than 10 mm in diameter is currently defined as an early breast cancer. Therefore, l is assumed to be the sample time with which the microwave penetrates through a tumor of 10 mm in diameter. The energy of point r can be obtained by taking the sum of the squares of the windowed signals as follows:

$$p_i(r) = \sum_{n_{\max}}^{n_{\max}+l} |x_i(r)\, h[n]|^2. \tag{10}$$

The energy vector of point r for 9 emitter antennas can be obtained as

$$\boldsymbol{p}(r) = [p_1(r),\ p_2(r),\ \ldots,\ p_9(r)]. \tag{11}$$

The spatial smoothing method is employed for the energy vector $\boldsymbol{p}(r)$, and the transformed matrix is

$$\boldsymbol{M}(r) = \begin{bmatrix} p_1(r) & p_2(r) & \cdots & p_6(r) \\ p_2(r) & p_3(r) & \cdots & p_7(r) \\ p_3(r) & p_4(r) & \cdots & p_8(r) \\ p_4(r) & p_5(r) & \cdots & p_9(r) \end{bmatrix}. \tag{12}$$

The DCRCB algorithm is applied again to the transformed matrix, and the final energy of point r, $\boldsymbol{p}(r)$, can be treated as pixels for image reconstruction.

The reconstructed image of the breast is obtained by scattering the point throughout the whole region and employing the beamformer output energy as the pixel of locations.

4. Results

In this section, the effectiveness of the DCRCB algorithm is demonstrated by applying it to the simulated backscattered signals. In the numerical study, the Debye parameters in Eq. (1) are for the normal breast tissue, for the chest wall, for the skin, and for the tumor.[19] Figures 6 and 7 show the reconstructed images created by the DCRCB algorithm, in which the impulse is emitted from 9 antennas in turn and the reflected waveforms are detected by the other 8 antennas. A tumor with a size of 2 mm in diameter is assumed to be located at (35, 40, 40) or (30, 60, 30).

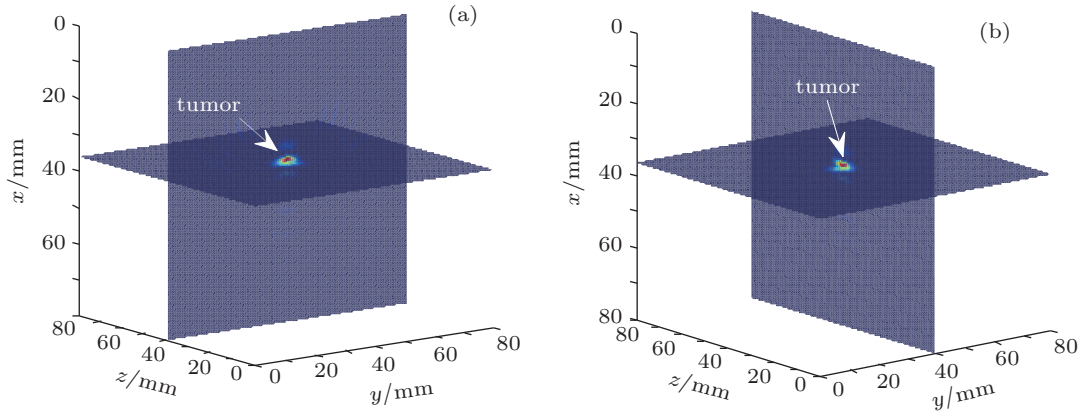


Fig. 6. (color online) The 3D reconstructed images of the breast in the case of a tumor with a size of 2 mm in diameter at the location of (35, 40, 40): (a) slices of x at 35 mm and z at 40 mm; (b) slices of x at 35 mm and y at 40 mm.

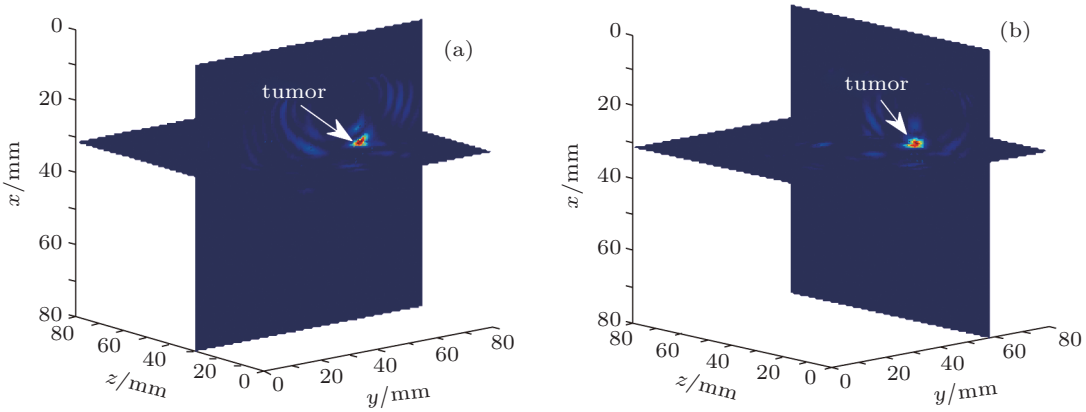


Fig. 7. (color online) The 3D reconstructed breast images in the case of a tumor with a size of 2 mm in diameter at the location of (30, 60, 30): (a) slices of x at 30 mm and z at 30 mm; (b) slices of x at 30 mm and y at 60 mm.

The highlight in the reconstructed image presents the correct information about the tumor embedded in the breast, and almost no noise influences the imaging results. The results also verify the robustness of the DCRCB algorithm when applied to breast image reconstruction.

5. Conclusion

The basic 3D planar structure of the breast configuration is applied to breast cancer detection with considerations of the skin, fat, tumor, glands, and the chest wall. The details of the DCRCB algorithm employed for the detection are presented. An assumed tumor with a size of 2 mm in diameter can be detected with the dispersive model and the influence of glands can be reduced by the DCRCB algorithm. The study demonstrates the good stability of the DCRCB algorithm and testifies the feasibility of UWB microwave imaging for early breast cancer detection. In our subsequent studies, more realistic breast models, such as the MRI-derived FDTD model, will be employed to verify the reliability of the image algorithm; and some essential experiments will be carried out to check the feasibility of this UWB image technology.

References

[1] Xu X H and Li H 2008 *Acta Phys. Sin.* **57** 4623 (in Chinese)
[2] Liu G D and Zhang Y R 2011 *Acta Phys. Sin.* **60** 4303 (in Chinese)
[3] Bond E J, Li X, Hagness S C and Van Veen B D 2003 *IEEE Trans. Antennas Propag.* **51** 1690
[4] Winters D W, Bond E J and Hagness S C 2006 *IEEE Trans. Antennas Propag.* **54** 3517
[5] Klemm M, Leendertz J A, Gibbins D, Graddock I J, Preece A and Benjamin R 2009 *IEEE Antennas Wirel. Propag. Lett.* **8** 1349
[6] Fear E C, Hagness S C, Meaney P M, Okoniewski M and Stuchly M A 2002 *IEEE Microwave Mag.* **3** 48
[7] Meaney P M, Fanning M W, Li D, Poplack S P and Paulsen K D 2000 *Microwave Theory Tech.* **48** 1841
[8] XiaoX and Kikkawa T 2008 *Appl. Surf. Sci.* **255** 597
[9] Xiao X and Kikkawa T 2008 *Jpn. J. Appl. Phys.* **47** 3209
[10] FearE Cand Stuchly M A 2000 *IEEE Trans. Microwave Theory Tech.* **48** 1854
[11] Berenger J P 1994 *J. Comput. Phys.* **114** 185
[12] Berenger J P 1996 *J. Comput. Phys.* **127** 363
[13] Gedney S D 1996 *IEEE Trans. Antennas. Propag.* **44** 1630
[14] Li X and Hagness S C 2001 *IEEE Microwave Compon. Lett.* **11** 130
[15] Xiao X and Kikkawa T 2008 *International Conference on Microwave and Millimeter Wave Technology*, April 21–24, 2008 Nanjing, China, p. 1707
[16] Stoica P, Wang Z S and Li J 2003 *IEEE Signal Processing Lett.***10** 172
[17] Guo B, Wang Y and Li J 2006 *J. Electromagnetic Waves Appl.* **20** 53
[18] Li J, Stoica P and Wang Z S 2004 *IEEE Trans. Signal Processing* **52** 2407
[19] Young J L 1995 *IEEE Trans. Antennas Propag.* **43** 422